MONITORING OIL SPILL PROGRESSION AND OIL SPILL VOLUME USING SATELLITE IMAGES

P. L. A. Hilario[1], R. M. de la Cruz[1], D. C. D. Vergara[1], A. J. Sabuito[1], N. J. Borlongan[1], J. I. Tabardillo[1]

[1] Philippine Space Agency, Quezon City 1109, Philippines –
paul.hilario@philsa.gov.ph, roel.delacruz@philsa.gov.ph, dhann.vergara@philsa.gov.ph, arlo.sabuito@philsa.gov.ph,
jomari.tabrdillo@philsa.gov.ph, noel.borlongan@philsa.gov.ph

KEY WORDS: Oil Spill, Oil thickness, Volume Calculation, SAR and Optical oil spill mapping, Sentinel Asia, Disaster Charter

ABSTRACT:

Satellite imagery is an indispensable tool in operational oil spills mapping. The smooth surface of oil sleeks make them visible in Synthetic Aperture Radar (SAR) imagery due to the low backscatter values making the oil spills distinctly dark in SAR images compared to the surrounding water. Oil extent delineation using SAR is very common but aside from using SAR images, optical satellite images are also of great help by capitalizing on the spectral characteristics of the oil surface to isolate the oil extents. The delineated extents are post-processed in a Geographic Information System (GIS) software where the oil spill area is calculated and published as oil extent maps. Though the area can be calculated, estimating the volume of oil present in the extent map remains to be a challenge. To answer this problem, this paper proposes a Physics-based solution to calculate the thickness of the oil by analysing local maxima in the reflectance spectrum of oil-covered water. Using this technique, oil thickness was estimated from Sentinel-2 multispectral images of an oil spill. It yielded an average oil thickness estimate of 0.560 ± 0.164 microns. The calculated thickness is used to estimate the volume of spilled oil.

1. INTRODUCTION

1.1 Oil Spill in Oriental Mindoro, Philippines

Last February 28, 2023, the MT Princess Empress carrying 800,000 litres of Industrial Fuel Oil was reported to be half submerged near Oriental Mindoro, Philippines (Figure 1). The ship was completely submerged and sunk on the next day (DENR, 2023). Five days after, spilled oil reached the shorelines triggering a massive coastal clean-up and ban on fishing activities (BFAR, 2023). The incident caused an estimated 7 billion Php (~126 Million USD) in damages to mangroves, sea grass, and coral reefs, and 3 Billion Php (~54 Million USD) in damages to agriculture (Santos, 2023).

1.2 Sentinel Asia activation and International Charter Space and Major Disasters Escalation

An Emergency Operations Request (EOR) to capture images on the oil spill area was immediately submitted to the Asian Disaster Reduction Centre (ADRC) through facilitated by the Japan Aerospace Exploration Agency (JAXA). The same request was escalated into the International Charter Space and Major Disasters to capture more images to help in monitoring and containment activities.

Figure 1. Oil spill location (in red dot).

2. OIL SPILL EXTENT MAPPING AND DISTRIBUTION

2.1 Optical and SAR Data

The following satellite images are used throughout the duration of Sentinel Asia and International Charter activation:

Satellite	Provider	Source	Maps
Sentinel-1A	European Space Agency (ESA)	International Charter	4
RCM-3	Canadian Space Agency (CSA)	International Charter	4
Gaofen-3	China National Space Administration (CNSA)	International Charter	4
RCM-1	Canadian Space Agency (CSA)	International Charter	4
Formosat-5	Taiwan Space Agency (TASA)	Sentinel Asia	2
Sentinel-2B	European Space Agency (ESA)	International Charter	4
Worldview-3	Digital Globe	International Charter	1
ALOS-2	Japan Aerospace Exploration Agency (JAXA)	Sentinel Asia	2
Tandem-X	German Aerospace Center (DLR)	International Charter	1
Landsat-8	US Geological Survey (USGS)	International Charter	1
SAOCOM-1B	Argentina National Space Activities Commission (CONAE)	International Charter	1
Landsat-9	US Geological Survey (USGS)	International Charter	1

Table 1. List of satellite image used and oil spill maps produced.

2.2 Oil Extent Mapping

The images received from Sentinel Asia and the disaster Charter were processed to produce the oil extent maps. Image segmentation was used due to misclassification in threshold-based and spectral-based processes. There is difficulty encountered when trying to set standardized threshold or indices operationally. This is due to effect of wind speed on water surface that affects the backscatter values from SAR images. Too low will deter the detection of oil spill because it makes the surface smooth. Too high and it would need very thick oil film to dampen or smoothen the surface. Detection on SAR images capitalizes on the dampening of capillary waves that makes the backscatter values low on dampened areas (Fingas, 2018) compared to the surrounding ocean water. They appear dark on SAR images an interpreted as oil slicks. But other areas also exhibit the same darkened characteristic on the ocean surface. Biogenic films produced by marine life can also cause the dampening effect (Jones, 2011). They need to be carefully removed from the delineation. To balance over-delineation or mis-delineation, confidence level is introduced. High, Medium, and Low confidence is added into the map to factor this uncertainty.

Due to the uniqueness of environmental situation at the time of each image was taken, it was determined that image segmentation was the fastest and most efficient method in extracting the oil spill extents.

The following process is implemented:

a.) An image is visually inspected to determine the location of likely oil spill.
b.) A subset of the image containing the areas with possible oil spills is extracted from the whole scene.
c.) Image segmentation is implemented to create objects with similar spectral, spatial, and textural characteristics. Some segmentation parameters are adjusted depending on the type and quality of satellite image.
d.) The segments are classified into four (4) classes namely, High Confidence oil, Medium Confidence oil, Low Confidence oil, and Non-oil objects.
e.) The final classification is exported to GIS software for layout and area calculations. Area is one of the main information released for this specific oil spill.

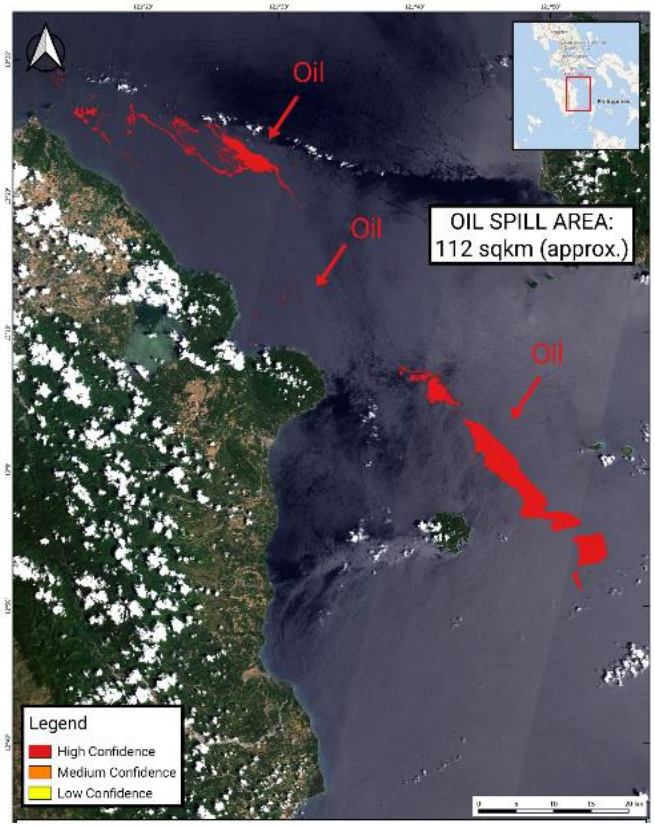

Figure 2. Example of oil extent map derived from Sentinel-2B optical satellite from ESA captured 23 March 2023. The oil extent in the image is approximately 112 square kilometres in area.

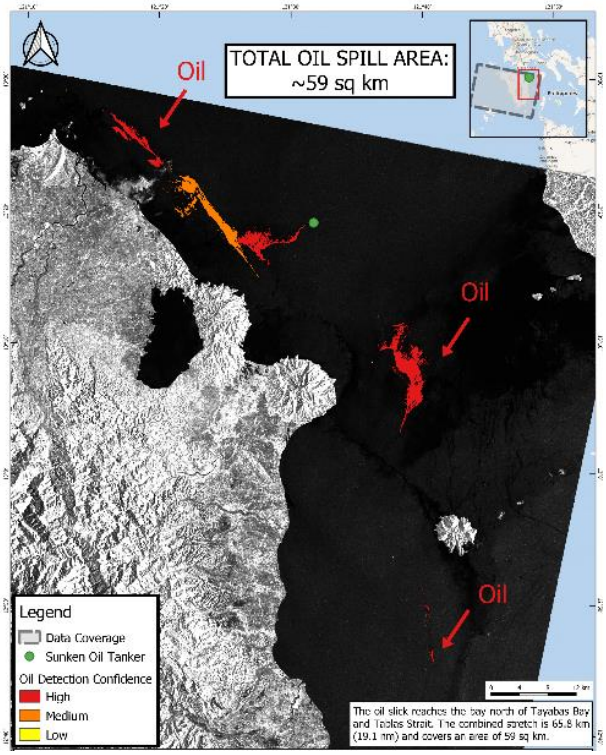

Figure 3. Example of oil extent map showing High and Low-confidence oil extents derived from Sentinel-1A SAR satellite from ESA captured 31 March 2023. The oil extent in the image is approximately 59 square kilometres in area.

The maps were produced from the images provided by disaster charter members. After closing of the disaster charter activation, free data from Sentinel-1, Sentinel-2, Landsat-8, and Landsat-9 were used continuously to monitor the oil spill.

2.3 Data Distribution

The oil extent maps were distributed to various agencies involved in the incident especially to the Department of Environment and Natural Resources (DENR), Office of Civil Defence (OCD) and its regional offices, Philippine Coast Guard (PCG), and members of the National Disaster Risk Reduction and Management Council (NDRRMC) through email. The same maps were also distributed to the public through official social media pages and press conferences.

3. ESTIMATING THE THICKNESS AND VOLUME OF THE OIL SLICK

Consider a uniformly thick oil of thickness t and refractive index n_{oil} on the surface of water (refractive index n_{water}) as shown in Figure 4. Sunlight is incident from air (refractive index n_{air}) at an angle of θ_i with respect to the oil surface normal.

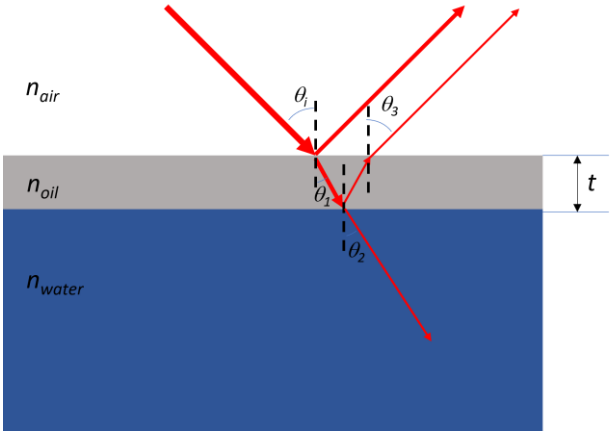

Figure 4. Thin film of oil over water.

Due to the change in the refractive index at the interface, light gets partially reflected at the air-oil interface, while some gets transmitted towards water. The transmitted light will also be partially reflected at the oil-water interface and transmitted into the oil-air interface. The reflection coefficients (Born and Wolf, 2013) for s-polarized (polarized perpendicular to plane of incidence) and p-polarized (parallel to plane of incidence) are given by

$$r_s = \frac{n_i cos\theta_i - n_t cos\theta_t}{n_i cos\theta_i + n_t cos\theta_t} \quad (1)$$

$$r_p = \frac{n_t cos\theta_i - n_i cos\theta_t}{n_t cos\theta_i + n_i cos\theta_t} \quad (2)$$

where θ_t is $n_i sin\,\theta_i = n_t sin\,\theta_t$
n_t is refractive index at the transmission side

Consider the system in Figure 4, at the first reflection, the incident side will be air while the transmission side will be oil. Consequently, at the second reflection the incident side will be that of oil while the transmission side will be that of water. Meanwhile, the transmission coefficients are given by

$$t_s = \frac{2n_i cos\theta_i}{n_i cos\theta_i + n_t cos\theta_t} \quad (3)$$

$$t_p = \frac{2n_i cos\theta_i}{n_t cos\theta_i + n_i cos\theta_t} \quad (4)$$

At the first reflection, the effective reflection coefficients are given by

$$r_{s1} = \frac{n_{air} cos\theta_i - n_{oil} cos\theta_1}{n_{air} cos\theta_i + n_{oil} cos\theta_1} \quad (5)$$

$$r_{p1} = \frac{n_{oil} cos\theta_i - n_{air} cos\theta_1}{n_{oil} cos\theta_i + n_{air} cos\theta_1} \quad (6)$$

Note that since the refractive index of oil is greater than that of air, the resulting reflection coefficients will be less than zero, indicating a π phase shift. The effective reflection coefficient at the second reflection is given by

$$r_{s2} = \frac{n_{oil} cos\theta_1 - n_{water} cos\theta_2}{n_{oil} cos\theta_1 + n_{water} cos\theta_2} \frac{4n_{oil} n_{air} cos\theta_i cos\theta_1}{(n_{air} cos\theta_i + n_{oil} cos\theta_1)^2} e^{i\frac{4\pi n_{oil} t}{\lambda cos\,\theta_1}} \quad (7)$$

$$r_{p2} = \frac{n_{water} cos\theta_1 - n_{oil} cos\theta_2}{n_{water} cos\theta_1 + n_{oil} cos\theta_2} \frac{4n_{oil} n_{air} cos\theta_i cos\theta_1}{(n_{oil} cos\theta_i + n_{air} cos\theta_1)^2} e^{i\frac{4\pi n_{oil} t}{\lambda cos\,\theta_1}} \quad (8)$$

where the phase shift $i\frac{4\pi n_{oil}t}{\lambda \cos\theta_1}$ is the phase shift due to the propagation along the thickness of the oil film.

Next consider an incident electric field given by $\overrightarrow{E_0} = E_{s0}\hat{s} + E_{p0}\hat{p}$, where $\hat{s}$ and $\hat{p}$ are the unit vectors along the *s* and *p* polarization directions. The *s* and *p* components of the reflected electric field, $\vec{E} = E_s\hat{s} + E_p\hat{p}$ will be the superposition of the two returning fields given by

$$\begin{aligned}\vec{E} &= \left(\frac{n_{air}cos\theta_i - n_{oil}cos\theta_1}{n_{air}cos\theta_i + n_{oil}cos\theta_1}\right. \\ &+ \left.\frac{n_{oil}cos\theta_1 - n_{water}cos\theta_2}{n_{oil}cos\theta_1 + n_{water}cos\theta_2}\frac{4n_{oil}n_{air}cos\theta_i cos\theta_1}{(n_{air}cos\theta_i + n_{oil}cos\theta_1)^2}e^{i\frac{4\pi n_{oil}t}{\lambda\cos\theta_1}}\right)E_{s0}\hat{s} \\ &+ \left(\frac{n_{oil}cos\theta_i - n_{air}cos\theta_1}{n_{oil}cos\theta_i + n_{air}cos\theta_1}\right. \\ &+ \left.\frac{n_{water}cos\theta_1 - n_{oil}cos\theta_2}{n_{water}cos\theta_1 + n_{oil}cos\theta_2}\frac{4n_{oil}n_{air}cos\theta_i cos\theta_1}{(n_{water}cos\theta_1 + n_{oil}cos\theta_2)^2}e^{i\frac{4\pi n_{oil}t}{\lambda\cos\theta_1}}\right)E_{p0}\hat{p}\end{aligned} \quad (9)$$

Lastly, the reflectance *R* is given by the ratio of the field intensity that is

$$R = \frac{|E_s|^2 + |E_p|^2}{|E_{s0}|^2 + |E_{p0}|^2} \quad (10)$$

Note that apart from the phase shifts due to propagation given by the exponentials, the refractive indices will also be dependent on wavelength, and hence the reflectance value will also be wavelength dependent. For a randomly polarized light given by described by the electric field $\overrightarrow{E_0} = \frac{1}{\sqrt{2}}\hat{s} + \frac{1}{\sqrt{2}}\hat{p}$, the reflected intensity is given by

$$\begin{aligned}R = &\left|\left(\frac{n_{air}cos\theta_i - n_{oil}cos\theta_1}{n_{air}cos\theta_i + n_{oil}cos\theta_1} + \right.\right. \\ &\left.\left.\frac{n_{oil}cos\theta_1 - n_{water}cos\theta_2}{n_{oil}cos\theta_1 + n_{water}cos\theta_2}\frac{4n_{oil}n_{air}cos\theta_i cos\theta_1}{(n_{air}cos\theta_i + n_{oil}cos\theta_1)^2}e^{i\frac{4\pi n_{oil}t}{\lambda\cos\theta_1}}\right)\right|^2\frac{1}{2} + \\ &\left|\left(\frac{n_{oil}cos\theta_i - n_{air}cos\theta_1}{n_{oil}cos\theta_i + n_{air}cos\theta_1} + \right.\right. \\ &\left.\left.\frac{n_{water}cos\theta_1 - n_{oil}cos\theta_2}{n_{water}cos\theta_1 + n_{oil}cos\theta_2}\frac{4n_{oil}n_{air}cos\theta_i cos\theta_1}{(n_{water}cos\theta_1 + n_{oil}cos\theta_2)^2}e^{i\frac{4\pi n_{oil}t}{\lambda\cos\theta_1}}\right)\right|^2\frac{1}{2}\end{aligned} \quad (11)$$

Since, the intensity of the incident electric field is *1*, the intensity in equation (11) will also be equal to the reflectance. Figure 5 shows the reflectance spectrum for various oil thicknesses.

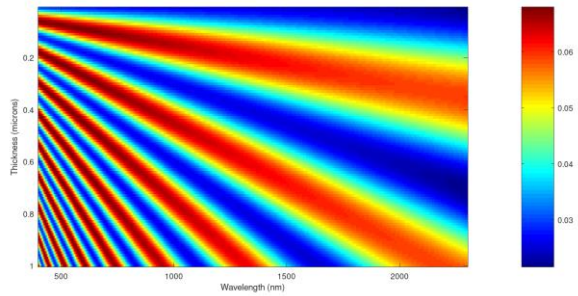

Figure 5: Reflectance spectrum for various oil film thickness at 30° incident angle

It may be observed that the spectrum changes as the thickness of the oil film thickness. This implies that the thickness of the film has a signature reflectance, which may be used to identify the thickness of the film. There is a peak if the phase shift between the interfering fields are integral multiples of 2π, that is

$$tan^{-1}\left(\frac{Im\{r\}}{Re\{r\}}\right) = 2m\pi \quad (12)$$

In the case of shown in Figure X, the phase shift come from reflecting from air to oil, described by equations (5) and (6), and the plane wave propagation within the oil film (equations (7) and (8)), this results to a phase shift given by

$$\frac{4\pi n_{oil}t}{\lambda\cos\theta_1} + \pi = 2m\pi \quad (13)$$

Which then allows for the estimation of the oil thickness based on the location of the spectral peaks. . This is similar to the results used in estimating the thickness in the microwave region (Fingas 2018; Hammoud et al, 2022, Hollinger, 1973). As described by Fingas (2018), the challenge with using using interference to estimate thickness remotely is that the thickness that will generate a maximum or a minimum at a particular wavelength is not unique. To be more specific of the thickness, multiple wavelengths will be required. This is inherent in multispectral imaging which captures images of the oil sleek at different wavelengths.

Note that equation (13) may be written as

$$\frac{1}{\lambda} = \frac{\cos\theta_1}{2tn_{oil}}m - \frac{\cos\theta_1}{4tn_{oil}} \quad (14)$$

Equation (14) is a linearized form of equation (13). Equation (14) shows the inverse of the wavelength, and the interference order *m* forms a linear relationship. More importantly the thickness of the film is related to the slope σ by

$$t = \frac{\cos\theta_1}{2n_{oil}\sigma} \quad (15)$$

A limitation is the maximum wavelength of the imaging sensor. At normal incidence, the maximum thickness that the method will be able to accurately estimate is given by

$$t_{max} = \frac{\lambda_{max}}{4\,n_{oil}} \quad (16)$$

where the λ_{max} is the central wavelength of the farthest band. This is also limited to the number of bands used. The higher the spectral resolution is, the better is the detection accuracy.

4. RESULTS AND DISCUSSION

Applying the estimated oil thickness into the maps produced from satellite images, volume can be then calculated. It should be noted that the volume estimates are only on those areas that were captured on the moment that the satellite took image. They do not include the continuous spills on other days where image were not available, those that reached the shores, and those that were not in the image coverage.

A sample spectral plot from a multispectral image using Sentinel-2 was taken of an oil spill in Occidental Mindoro, Philippines from February 2023, in particular, an image of the oil spill on March 23, 2023.

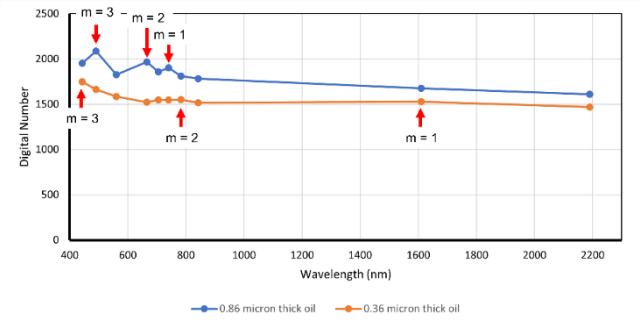

Figure 6: (Top) Oil spill regions identified from Sentinel 2 image Oriental Mindoro. (Bottom)Reflectance spectrum at the selected regions of interest in the multispectral image of the 2023 Mindoro oil spill. Peaks are identified as the local maxima of the spectrum. For the region with thick oil, the peaks were identified to be at 490 nm, 665 nm, and 740 nm. Whereas for the thin oil, the peaks were identified to be at 443 nm, 783 nm, and 1610 nm.

In this study, the oil sleeks were identified by remote sensing expert from the image. The thickness of a total of 12 points in the image were calculated by performing a linear regression following the linear equation shown in equation (14). Sample linear regression plots are shown in Figure 6 The results are shown in Table 2.

Position Number	Slope	y-intercept (μm^{-1})	Thickness (μm)
1	0.34	0.94	0.86
2	0.43	0.70	0.70
3	0.76	0.51	0.39
4	0.43	0.70	0.70
5	0.44	0.24	0.67
6	0.85	0.33	0.35
7	0.51	0.17	0.59
8	0.50	0.13	0.59
9	0.82	-0.25	0.36
10	0.82	-0.25	0.36
11	0.53	0.53	0.55
12	0.49	0.67	0.61
Average			**0.560**
Standard deviation			**0.164**

Table 2. Thickness estimates at various points in the multispectral image. noil is assumed to be 1.45.

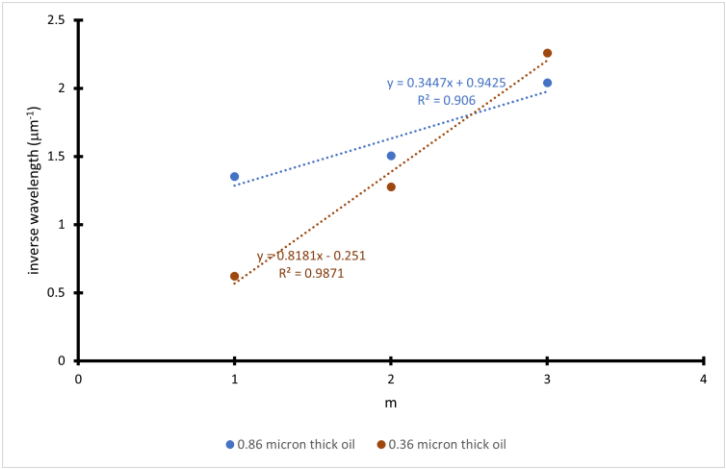

Figure 7: Sample linear regression plots for the spectral peak location vs interference order of reflectance spectra of thick and thin oil.

The calculated average thickness is *0.56 μm ± 0.164 μm*. Area estimates of the oil spill shown in Figure Z results to an area of *112 km²*. The volume estimate at this area is *62.74 kL ± 9.79 kL*. Figure 8 shows the estimated volume from March 1, 2023 to March 31, 2023

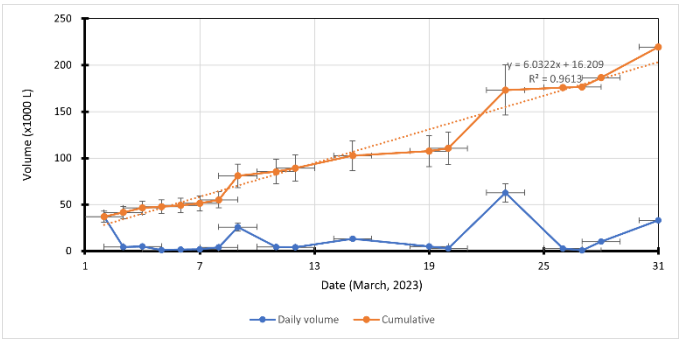

Figure 8: Daily and cumulative volume estimate from satellite images

The cumulative volume is the sum from March 1, 2023, up until the current date. While this may overestimate the actual volume, this value can provide for an upper bound of the volume of oil sleek detected by satellite imaging. In terms of response operations, this can provide a minimum value of what remains to be released from the source, an upper bound of the rate of release, and the minimum area of the potential spread.

CONCLUSION AND RECOMMENDATIONS

The proposed methodology in calculating volume of spilled oil can provide a good estimate on how much oil has been released from the sunken vessel. Though satellite-based oil spill mapping can't provide continuous imaging of the site, available satellite data can provide an insight on how much oil has been released and how much more to expect. Until March 31, the estimated volume based on available images was estimated to be around 230,000 litres (Figure 8). This indicates that there are much more to expect if the source can't be contained.

ACKNOWLEDGEMENTS

The oil spill mapping and monitoring activities in this paper was made possible by the support of the JAXA, ADRC, the International Charter Space and Major Disaster.

REFERENCES

BFAR 2023, BFAR Oil Spill Bulletin No 3. Oriental Mindoro and Caluya, Antique Oil Spill Bulletin No. 03 Series of 2023. https://www.bfar.da.gov.ph/2023/04/26/oriental-mindoro-and-caluya-antique-oil-spill-bulletin-no-03-series-of-2023. (30 April 2023)

Born, Max, and Emil Wolf, 2013. Principles of optics: electromagnetic theory of propagation, interference and diffraction of light. *Elsevier*.

DENR 2023, Situational Report No. 25. https://www.denr.gov.ph/images/Mindoro_Oil_Spill/Sitrep_No._35_Apr_25.pdf (30 April, 2023)

Fingas, M., 2018. The Challenges of Remotely Measuring Oil Slick Thickness. *Remote Sensing*, 10 (2), 319.

Hammoud, Bilal, Georges Daou, and Norbert Wehn. 2022. "Multidimensional Minimum Euclidean Distance Approach Using Radar Reflectivities for Oil Slick Thickness Estimation" *Sensors* 22, no. 4: 1431. https://doi.org/10.3390/s22041431

Hollinger, J. P., and R. A. Mennella, 1973 "Oil spills: Measurements of their distributions and volumes by multifrequency microwave radiometry." *Science* 181.4094 (1973): 54-56.

Jones, C. E., Minchew, B., & Holt, B., 2011. Polarimetric decomposition analysis of the Deepwater Horizon oil slick using L-band UAVSAR data. *International Geoscience and Remote Sensing Symposium.* https://doi.org/10.1109/igarss.2011.6049663

Santos, J, 2023, Mindoro oil spill's potential damage to environment at P7B —DENR. https://www.bfar.da.gov.ph/2023/04/26/oriental-mindoro-and-caluya-antique-oil-spill-bulletin-no-03-series-of-2023 (30 April, 2023)